CHALMERS

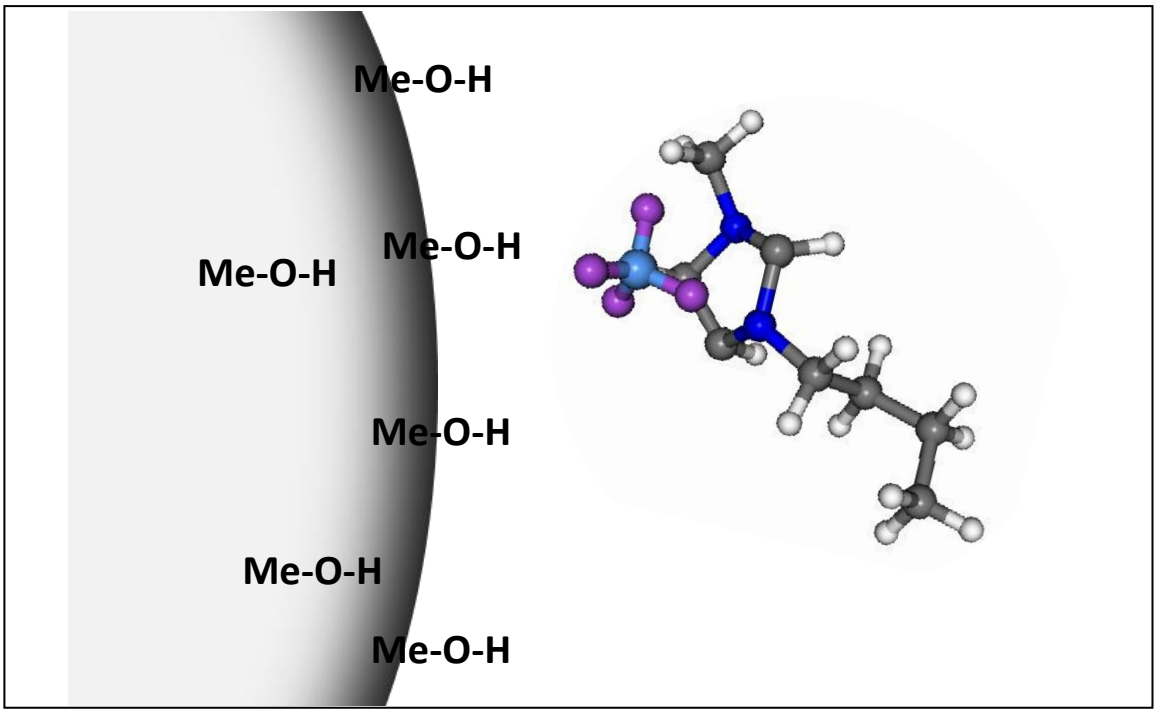

Colloidal interactions in ionic liquids:
Effect of surface area and particle type

Thesis for the Degree of Erasmus Mundus Master in Nanoscience and Nanotechnology.

LUIS ANTONIO AGUILERA MEDINA

Department of Applied Physics
Condensed Matter Physics Group
CHALMERS UNIVERSITY OF TECHNOLOGY
Göteborg, Sweden, 2011

Education and Culture DG
ERASMUS MUNDUS

Colloidal interactions in ionic liquids:

Effects of surface area and particle type

Luis Antonio Aguilera Medina

Department of Applied Physics

Chalmers University of Technology

Göteborg, Sweden, 2011.

Colloidal interactions in ionic liquids:

Effects of surface area and particle type

Luis Antonio Aguilera Medina

Department of Applied Physics

Chalmers University of Technology

SE-412 96 Gothenburg

Sweden

Telephone: +46 (0) 31 772 1000

Colloidal interactions in ionic liquids:
Effects of surface area and particle type

Luis Antonio Aguilera Medina
Department of Applied Physics, Chalmers University of Technology

Abstract

The increasing demand for batteries with high energy and power density, yet at the same time reliable and safe, has challenged the researchers to look for new materials. Ionic liquid gels have emerged as a suitable electrolyte candidate given the improved mechanical properties provided by the gels and the high ionic conductivity, non-flammability, low vapor pressure, and wide thermal stability from the ionic liquids.

In this work, dispersions of silica (SiO_2), alumina (Al_2O_3), and titania (TiO_2) nanoparticles in 1-butyl-3-methylimidazolium tetrafluoroborate (BMIM-BF_4) ionic liquid were studied. The silica and alumina nanoparticles form gels at concentrations between 5 and 7.5 wt%, whereas the titania nanoparticles simply sediment. Despite the solid-like behavior (gel), the ionic conductivity and glass transition temperature remains relatively unchanged with respect to that of the pure BMIM-BF_4. However, for low nanoparticle concentration a small increase in conductivity is observed for all dispersions, whereas with increasing concentration the conductivity drops below that of the pure BMIM-BF_4. Dispersions with silica nanoparticles form stronger gels compared to those of alumina nanoparticles. The stabilization and interaction mechanisms present in the dispersions are discussed in function of the surface area, the nanoparticle hydrodynamic diameter, the surface charge, and the surface functional groups.

Keywords: Ionic liquids, gels, electrolytes, BMIM-BF_4, ionic conductivity, glass transition temperature, nanoparticles, silica, alumina.

TABLE OF CONTENTS

ABSTRACT **3**

1 INTRODUCTION **5**

2 COLLOIDAL SYSTEMS **7**

3 IONIC LIQUIDS AND IONIC LIQUID DISPERSIONS **9**

3.1 Ionic liquids....9

3.2 Ionic liquid suspensions and gels 11

4 MATERIALS AND METHODS **14**

4.1 Nanoparticles 14

4.2 Ionic liquid 16

4.3 Sample preparation....17

4.4 Experimental techniques....18
4.4.1 Differential scanning calorimetry 18
4.4.2 Photon correlation spectroscopy 20
4.4.3 Dielectric spectroscopy 24
4.4.4 Instruments and experimental conditions....27

5 RESULTS AND DISCUSSION **29**

5.1 Gelling point 29

5.2 Particle size....34

5.3 Ionic conductivity and glass transition temperature 36

6 CONCLUSIONS **40**

FURTHER WORK **41**

ACKNOWLEDGEMENTS **42**

BIBLIOGRAPHY **43**

Chapter 1

Introduction

The constant improvement of energy storage technologies has pushed current materials to their limits. In the specific case of Lithium batteries, there is a great interest for applications in electric vehicles [1-4]. Nevertheless, due to safety issues and reliability problems of currently used electrolytes, the development of such batteries has been slowed down [5-9]. One attractive solution emerges from the interesting properties of ionic liquids. Due to their high thermal stability [10, 11], low vapor pressure [11, 12], high ionic conductivity [13, 14], and non-flammability [15] ionic liquids are good candidates for battery electrolytes.

The use of ionic liquids as electrolytes in energy applications has been the topic of intense research in the last years, and different alternatives have been explored [16-19]. A particular case that is worth mentioning is the use of ionic liquid gels [16, 20]. They combine the thermal and electrochemical stability of ionic liquids over a wide temperature range with the mechanical properties of the gel. This eliminates the need of separator materials and leakage problems with liquid electrolytes are suppressed.

One possible way to gel ionic liquids is by using nanoparticles as gelling agents [20]. Several studies in this direction have been presented, characterizing the physical properties of ionic liquid gels [20, 21]. However the mechanisms involved in the gelation process are not completely understood. It is known that mechanism such as electrostatic repulsion, steric hindrance, or solvation forces play a role in the stabilization of colloidal systems, but depending on the characteristic of the continuous medium and the gelling agents some mechanism will dominate and determine the stability of the system [20, 22, 23]. In the case of ionic liquid gels this is not well understood, therefore, new studies have to be pursued.

In this thesis, the colloidal interactions in ionic liquid suspensions and gels are investigated by varying the nanoparticle type, size, and surface area. The influence on the gelling point and on properties such as ionic conductivity and glass

transition temperature are studied. We presume that by understanding the way the nanoparticles and the ionic liquids interact, it is possible to select the most suitable candidates for future electrolytes.

The thesis is structured in a way that the reader can familiarize with the topic of research and the actual needs in this field. In the first chapter, a brief introduction to the actual needs in the battery field is given, and a possible solution through the use of ionic liquid gels is proposed, together with the advantages of this novel system and a proposed method of investigation. In the second chapter, some general concepts and definition of the systems to be studied are provided in order to be able to understand the special way in which these systems behave and to understand the mechanism involved. In the third chapter, the actual status of the research on ionic liquid suspensions and gels is presented, in order to help us to further understand how ionic liquids gels behave. In the fourth chapter, the materials used are described, followed by the procedure in the sample preparation. Some theoretical background of each of the experimental techniques is provided. Moreover, the interpretation of the data obtained from the different techniques is also explained. In the fifth chapter, the results of this thesis are analyzed, discussed, and compared with previous works. Finally in the sixth chapter, the conclusions of the thesis are presented, followed by some remarks and further work.

Chapter 2

Colloidal systems

A colloidal dispersion is a system in which particles (dimension roughly between 1nm and 1μm) of any nature (solid, liquid, or gas) are dispersed in a continuous phase of a different composition (or state) [24]. Depending upon the state of the dispersed phase and the dispersion medium, eight different types of colloidal dispersions can be identified, see Table 1.

Table 1. Different types of colloidal dispersions.

Dispersed phase	**Dispersion medium**		
	Solid	**Liquid**	**Gas**
Solid	Solid sol or solid suspension	Sol or colloidal suspension	Solid aerosol
Liquid	Gel	Emulsion	Liquid aerosol
Gas	Solid foam	Foam	Do not exist

Due to the small size of the dispersed particles, colloidal dispersions are characterized by an extremely high interfacial area. Why do the particles not aggregate to reduce this interfacial energy? And which are the mechanisms working to stabilize these systems? This thesis work focuses on the mechanisms involved in stabilizing colloidal suspension and the sol-gel transition with increasing particle concentration.

In order to understand the stability of colloidal suspensions we first have to know the forces present in the system. Let us think for instance on gravity. Depending on the density difference between the particles and the fluid, the particles will either rise to the surface or sediment. In order to overcome these problems one could think about matching the densities of the particles with the liquid, but also think about reducing the size of the particles in such a way that gravity is overcome by the Brownian motion of the particles. In colloidal suspensions the particles can be stabilized due to forces of different nature, e.g.

electrostatic, steric, and solvation forces. In the case these stabilization forces are not strong enough; the particles will aggregate due to van der Waals interactions, depletion forces, or hydrogen bonding [25].

A gel is a combination of a fluid and a non-fluid colloidal or polymer network that expands throughout the whole volume of the fluid [26]. Gels can be classified in two classes, depending on the nature of the bonds/interactions in the network.

- Chemical gels. - The bonds between the subunits are chemical covalent bonds. Example: epoxy resins.
- Physical gels. – The bonds between the subunits are physical interactions. Example: gelatins.

Physical interactions between subunits can be broken by increasing temperature. This is why; physical gels are sometimes called thermoreversible gels.

In the same way that there are different way to stabilize a colloidal suspension (sol), there are different bonding mechanisms that can interact to form the colloidal network in the gel state. Some of the bonding mechanisms are: hydrogen bonding, hydrophobic interactions, helix formation, and ionic interactions [27]. Depending on the characteristics of the system, different stabilization mechanism could be working. A complete understanding of these mechanisms is necessary to have control of the gelation process (sol-gel transition at the gel point [26]) which is of importance for the implementation of a particular gel in future technologies.

Chapter 3

Ionic liquids and ionic liquid dispersions

3.1 Ionic liquids

Ionic liquids are liquids that consist exclusively of ions. This definition includes liquids that are known as molten salts which have high melting temperatures. However, in the last decades the term “ionic liquid” has been limited to those molten salts which have melting points below 100 °C [28]. Among the general properties of the ionic liquids, it is worth to mention the high thermal stability [10, 11], low vapor pressure [11, 12], wide temperature range stability as liquids, non-flammability [15], wide electrochemical window, and high ionic conductivity [13, 14, 28].

It is well known that by increasing the size of the ions and making them asymmetric, it is possible to decrease the melting temperature [28]. This is easily explained as follows: given the nature of the ions in ionic liquids, they tend to attract each other due to electrostatic forces. If the ions are small and symmetric, as in the case of sodium chloride, the ions will be close to each other and interact strongly. Moreover, due to their symmetry, the formation of crystals is favorable. If the size of the ions is increased, the distance between them will increase and as a result the electrostatic attractive force will decrease. In this way the melting point of the ionic liquid can be controlled. Furthermore, if the ions are asymmetric, the melting point can be diminished even more or eventually be suppressed. In Table 2 examples of different salts/ionic liquids and their respective melting points are presented. Some examples of typical anions and cations which are commercially available are shown in Figure 1. The versatility of the ionic liquids lies in that it is possible to synthesize thousands of them by simply varying a functional group, and such variation will determine the final macroscopic characteristics of that ionic liquid.

Table 2. Salts/ionic liquids and their respective melting point.

Salt/Ionic Liquid	Melting temperature (°C)
Sodium Chloride (NaCl)	800
Cesium Chloride (CsCl)	645
1-Butyl-3-Methylimidazolium Chloride (BMIM-Cl)	65
1-Butyl-3-Methylimidazolium Tetrafluoroborate (BMIM-BF_4)	-75

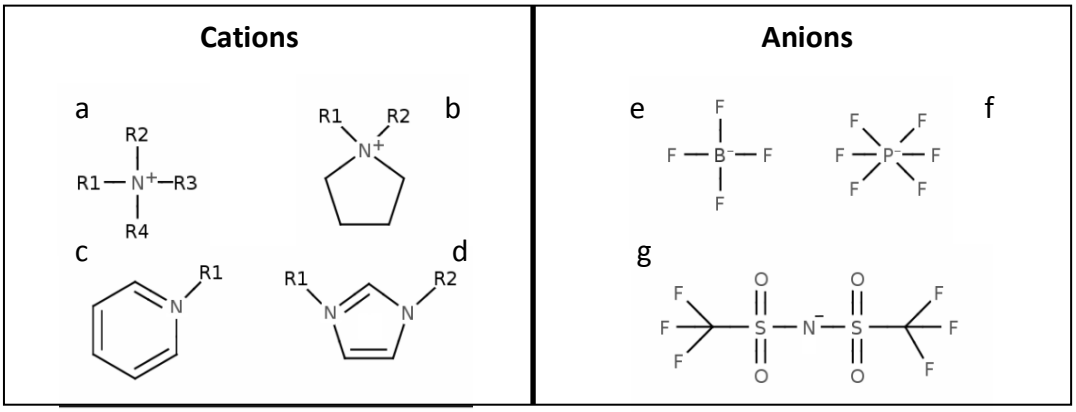

Figure 1. Examples of some typical ionic liquid cations and anions:
a) tetralkylammonium, b) N-alkyl-N-alkylpyrrolidinium, c) 1-alkylpyridinium, d) 1-alkyl-3-akylimidazolium, e) tetrafluoroborate, f) hexafluorophosphate, and g) bis(trifluoromethanesulfonyl)imide.

In the last years, ionic liquids have found different applications, e.g. as electroplating solvents, catalyzers, and electrolytes [19]. For the specific case of electrolytes, the interest in ionic liquid has greatly increased and already some possible applications are found in solar cells [16, 29], fuel cells [30], and lithium-ion batteries [21, 31]. Despite the already mentioned qualities of the ionic liquids, they are relatively new as electrolytes, and as such, there are draw backs, such as, toxicity, compatibility with the actual materials used, production cost, and all the problems that come with the introduction of a new technology.

3.2 Ionic liquid suspensions and gels

In electrolytes, the control of the physical properties is of great importance. As an example we have the viscosity. It is desirable to have a higher viscosity, if possible a gel, without deteriorating the ion conduction properties. An interesting approach taken by some research groups is the use of colloidal particles as gelling agents [20, 22]. Due to the high surface area, the relative low cost and the possibility of functionalize their surface; they are an attractive option.

Colloidal suspensions can be stabilized by means of electrostatic repulsion in aqueous and organic media. Nevertheless for the case of ionic liquids, due to the high ionic concentration, the electrostatic forces are screened, which might lead to particle aggregation [23]. However, it has been found that negatively charged silica nanoparticles can remain stable when dispersed in some ionic liquids [22]. Key properties of nanoparticles which might influence the colloidal stabilization are particle size, surface area, or surface functional groups.

One possible stabilization mechanism is the so called solvation force. It is known that some liquids when confined between flat surfaces can form layered structures. The resulting force from this layering mechanism has been studied in several molecular liquids [32-35]. In more recent studies, a similar mechanism has been identified in ionic liquids using atomic force microscopy [36, 37], surface force apparatus [38-41], and computational simulations [42, 43]. Interesting enough, the measured force corresponding to the stable layers appears to be in good agreement with the expected size of the ions. Compared to typical molecular liquids, ionic liquids tend to form layers even in the absence of confinement [44]. Given the structural properties of ionic liquids and the ability of strong interaction with charged surfaces; the formation of layers is facilitated. In this way, it has been proposed that the solvation force might be playing an important role in the stabilization of charged nanoparticles when suspended in ionic liquids [44, 45].

The use of functional groups on the surface of the nanoparticles is another way of stabilize the colloidal systems. In order to have strong repulsive forces due to excluded volume effects, it is necessary to have a high surface concentration and

low molecular weight of grafted polymers. Also if the polymer chains are not soluble the particles will tend to aggregate [12]. Another suggested stabilization mechanism, due to the characteristics of some ionic liquids, is the possibility for them to interact via hydrogen bonding with surface groups of the nanoparticles [16]. If the ions are bulky enough, the effect due to steric hindrance might be then strong enough to stabilize the colloidal system. If the concentration of nanoparticles is high enough, the stabilization forces will not be strong enough and as a result the particles will aggregate, forming a gel.

The term “ionic liquid gels” is given to gel systems where the fluid contained in the network is an ionic liquid. The use of silica nanoparticles as gelling agents in ionic liquids has previously been reported [20, 22, 45]. Interestingly enough, the ionic conductivity of these ionic liquid gels, compared to the pure ionic liquids, does not decrease considerably [20]. Due to the low concentration of the nanoparticles, the ionic liquids still has enough space to move through the network and therefore the conducting properties are not affected by the change in viscosity of the dispersion. The small decrease in ionic conductivity is explained by a weak interaction that exist between the ionic liquid and the nanoparticles, leading to a decrease of the mobility with an increase in particle concentration [20]. It has been proposed that hydrogen bonding between the silica nanoparticles and the ionic liquid might be playing an important role in this ionic mobility reduction [16, 20]. Furthermore, rheological studies have shown that by increasing particle concentration it is possible to increase the yield stress, leading to favorable mechanical properties without compromising the high ionic conductivity [20].

Another important factor determining the mechanical properties is the surface functional groups of the nanoparticles. Studies performed by Watanabe et al. showed a different rheological response if the nanoparticles were hydrophilic or hydrophobic [22]. For the former particles a mixed contribution of hydrogen bonding and van der Waals interactions are present, whereas for the latter only the van der Waals interactions contribute [22]. For hydrophilic nanoparticles the elastic modulus is higher for any given concentration than for the hydrophobic ones which can be ascribed to the hydrogen bonding contribution [22].

In this work we focus on a specific ionic liquid (BMIM-BF_4). The reason for choosing this particular ionic liquid comes from the extraordinary high concentration of silica nanoparticles that this ionic liquid can uptake before gelling. The values reported in literature reach up to 15 wt% [22]. Also, it has been reported that this system interacts via hydrogen bonding with the surface groups of the nanoparticles which is probably the reason of the high colloidal stability [16]. Furthermore, the formation of solvation layers has been confirmed for the case of BMIM-BF_4 on silica surfaces [41]. However, despite the numerous investigations regarding BMIM-BF_4 there are still some incongruences, for instance different gelling concentrations have been reported [16, 22], about the way the colloidal dispersions are stabilized, and the mechanisms involved.

Chapter 4

Materials and methods

4.1 Nanoparticles

The nanoparticles were donated by Evonik Industries with the exception of the silica nanoparticles of 400 m^2/g surface area that were purchased from Sigma-Aldrich Corporation. The nanoparticles used, together with their most interesting properties, are shown in Table 3.

Table 3. General properties of the nanoparticles used.

Nanoparticles	**Formula**	**Surface area (m^2/g)**	**Primary particle size (nm)**	**pH in 4% dispersion**
Aerosil-200	SiO_2	200±25	12	3.7-4.7
Sigma-Aldrich-400	SiO_2	400±40	7	3.7-4.3
Aeroxide-Alu C	Al_2O_3	100±15	13	4.5-5.5
Aeroxide-TiO-P25	TiO_2	50±15	21	3.5-4.5

The nanoparticles can be either hydrophilic or hydrophobic depending on the surface treatment that is given to them. For all nanoparticles used during this research work, none of them had a special treatment and therefore all of them are considered as hydrophilic.

All used nanoparticles have a fractal structure resulting from the synthesis method. In Figure 2 a schematic view of the nanoparticles and the bonding between them is shown. In the preparation process primary particles melt together to form a fractal structure, which gives rise to a high surface area [46]. By changing the primary particle size it is possible to tune the surface area. The fractal nanoparticles can interact with each other through hydrogen bonding and van der Waals forces.

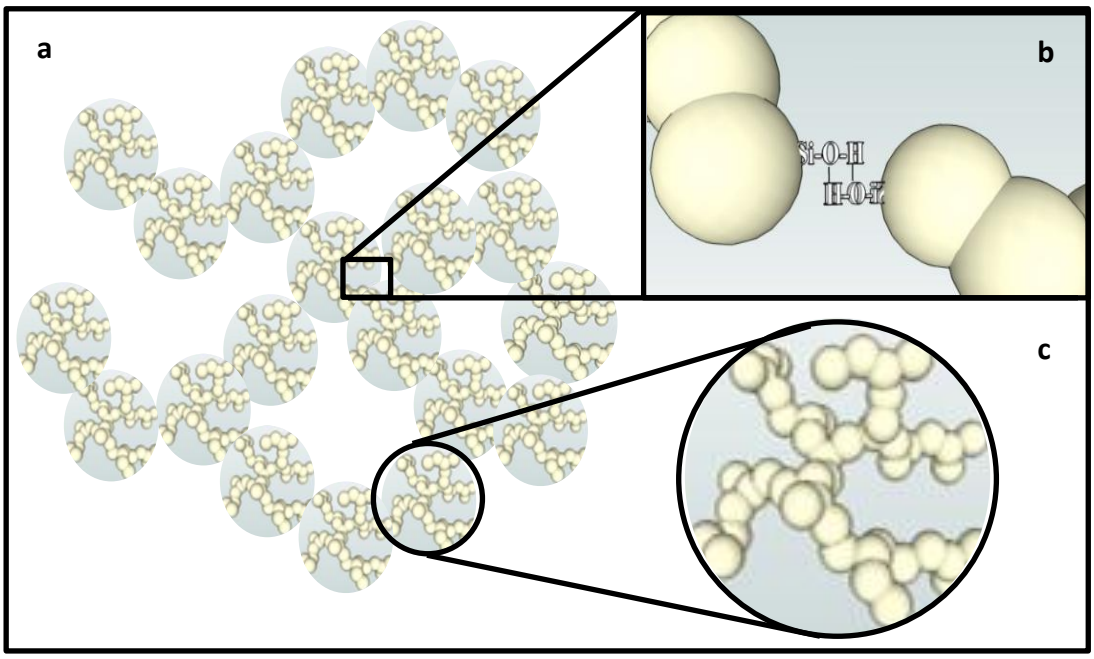

Figure 2. In this figure in a) an agglomerate of nanoparticles, b) the possible bonding between nanoparticles and c) a single nanoparticle are shown.

In the specific case of the silica nanoparticles the two basic groups that can be found on the surface are silanol and siloxane groups. These groups give the possibility of hydrogen bonding and a negatively charged surface [47, 48]. The groups are schematically represented in Figure 3.

Figure 3. Basic surface groups on silica nanoparticles.

For the case of the alumina nanoparticles there are three basic surface groups and these groups provide the possibility of a positive charge on the surface [47-51] as well as hydrogen bonding. In Figure 4 the surface groups on the alumina nanoparticles are shown.

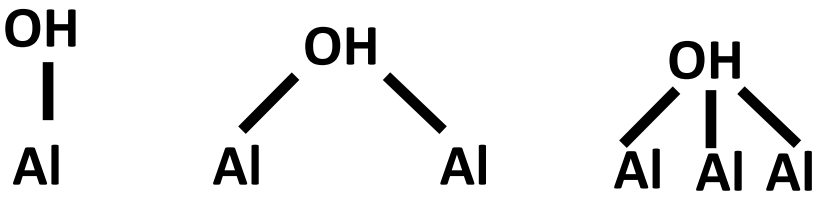

Figure 4. Surface groups of the alumina nanoparticles.

4.2 Ionic liquid

The ionic liquid use in this work is 1-butyl-3-methylimidazolium tetrafluoroborate, commonly referred to as BMIM-BF_4. The cation consists of an imidazole ring with butyl and methyl side groups, while the anion is tetrafluoroborate. The BMIM-BF_4 was purchased from Sigma-Aldrich Corporation. In Figure 5 the structure of the two ions is presented.

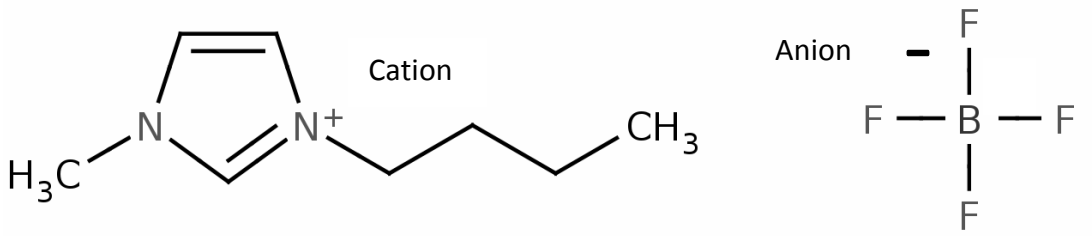

Figure 5. The structure of the two ions in BMIM-BF_4.

This ionic liquid have been widely study, therefore information such as conductivity, viscosity, and glass transition temperature can easily be found in literature [13, 14, 52, 53]. In Table 4 some properties of BMIM-BF_4 are presented. In the first row, the data measured in this work is reported, in the second row, the data obtained from literature are given.

Table 4. Some properties of BMIM-BF_4

Formula	**Molecular weight**	**Tg (K)**	**Conductivity RT (S/m)**	**Viscosity RT (mPa.s)**	**Heat Capacity RT (J/K.mol)**
$C_8H_{15}N_2BF_4$	226.02	186	0.11	**x**	**x**
Literature Values	**x**	188 [52]	0.35 [13, 52]	99 [54]	364 [55]

The properties of the ionic liquids strongly depend in variables such as purity, water content, and temperature; therefore some values may differ depending on the conditions [13, 54-57].

4.3 Sample preparation

The sample preparation was performed inside a glove box with an Argon environment. Prior to the sample preparation, the nanoparticles were dried for 24 hours in vacuum at 150 °C. The ionic liquid was used as received. All the equipment and vials used were thoroughly cleaned with isopropanol. The dried nanoparticles and the ionic liquid were kept inside the glove box at all times.

The sample preparation for all dispersions followed the same procedure. The nanoparticles and ionic liquid were weighed and mixed inside the glove box. Afterward the samples were taken out of the glove box, sealed with parafilm and put into an ultra-sonic bath for periods of 15 minutes for a minimum of 2 hours until achieving a uniform dispersion. After the ultrasound bath the samples were stored under ambient conditions until the respective experiments were performed. The time before measurements, vary from 4 to 8 weeks, depending on the availability of the equipment.

The nanoparticles concentration was systematically varied from low to high concentrations until the sample gelled. Once the sample gelled a more refined search of the gelling point was done.

Prior to the differential scanning calorimetry and dielectric spectroscopy experiments, the samples were sonicated for at least 30 minutes to avoid any aging effect (sedimentation, agglomeration). The samples for these experiments were loaded inside the glove box. In the case of photon correlation spectroscopy, the concentration of nanoparticles needed to be really low, well dispersed and in special vials. Therefore the samples were prepared just before the measurement and treated in ultra-sound for at least 3 hours.

4.4 Experimental techniques

In this section a brief introduction to the experimental techniques is given. For each experimental technique a description of the measurements of interest and the basic theory behind is explained. Also some specifications on the sample preparation is given.

4.4.1 Differential scanning calorimetry

The differential scanning calorimetry (DSC) is one of the most widely used thermal techniques. The DSC measures the energy changes that occur as a sample is heated, cooled or held isothermally, together with the temperature at which these changes occur. These energy changes enable the user to find and measure the transitions that occur in the sample quantitatively, and to note the temperature where they occur. With this information is possible to characterize materials for melting processes, glass transitions, crystallizations and a range of more complex events. An advantage of DSC is that the sample preparation is very simple, usually with little or no preparation; therefore measurements can be made quickly and easily.

The equipment used in this thesis work was a DSC-Q1000, TA Instruments. This equipment measures the heat flow as a function of temperature or time, where the actual value of heat flow measured depends upon the reference; therefore, it is not absolute. Both, the sample and the reference, are maintained at nearly the same temperature throughout the experiment. The reference sample (in this case an aluminum pan) should have a well-defined heat capacity over the range of temperatures to be scanned. Two different conventions exist for the display of the heat flow curve: one shows exotherms (release of energy from the system) in the downward direction and the other upward. In this thesis we will take the exotherms upward convention.

Figure 6 shows a typical DSC thermogram, where the most common transitions are depicted. The glass transition is represented as a step, whereas the melting and crystallization transitions are represented as peaks, but with different directions due to the nature of the transitions (exothermic or endothermic).

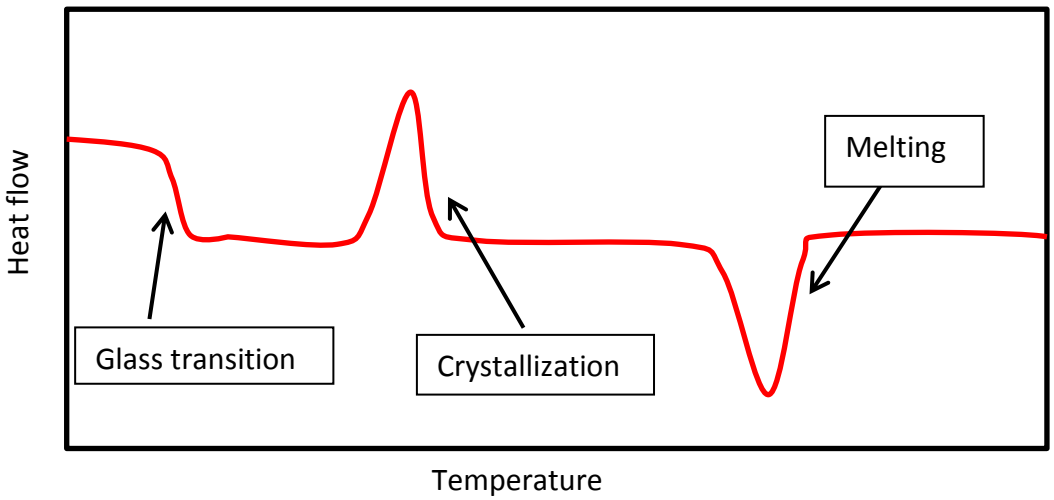

Figure 6. A typical DSC thermogram.

From the transitions shown in Figure 6, the glass transition temperature (T_g) is the one studied in this thesis. T_g is the temperature assigned to a transition above which amorphous (non-crystalline) materials are fluid and below which they are immobile and rigid, simply frozen in a disordered, non-crystalline glassy state.

The glass transition occurs over a region in temperature. Because of this, it is important to specify how T_g was determined. There are several conventions, but the most widely used are the onset, midpoint, and endpoint of the glass transition. To define these three points, two tangents to the baselines are drawn (before and after the transition) then a tangent to the point of highest derivate during the transition is drawn, these three lines together will define the points of interest, see Figure 7. During this thesis work, the onset convention will be the one used. For any further doubt, the reader is suggested to consult reference [58].

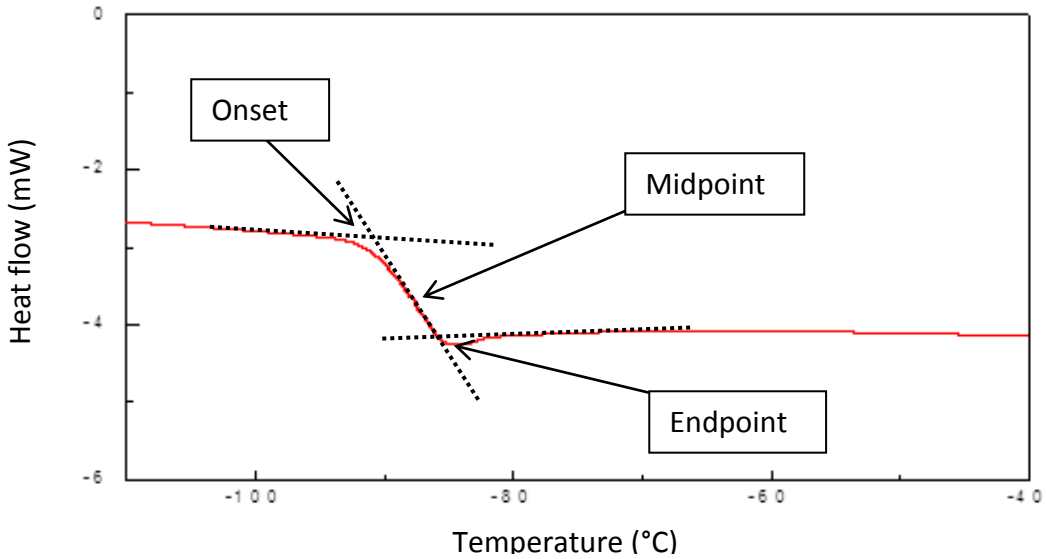

Figure 7. Glass transition and the different criteria to determine T_g.

4.4.2 Photon correlation spectroscopy

Photon Correlation Spectroscopy (PCS), sometimes referred to as Dynamic Light Scattering, is a technique that can be used to determine the size of particles typically in the sub-micron region [59].

In PCS Brownian motion is measured and related to the size of the particles. Brownian motion is the random movement of particles due to the bombardment by the solvent molecules that surround them. The larger the particle, the slower the Brownian motion will be. The diameter that is obtained by this technique is the diameter of a sphere that has the same translational diffusion coefficient as the particle, hence the name hydrodynamic diameter. The translational diffusion coefficient will depend not only on the size of the particle, but also on any surface structure, as well as the concentration and type of ions in the medium or even the shape of the particles [59].

PCS measures the rate at which the intensity of the scattered light fluctuates. In a system of particles, a speckle pattern (a random intensity pattern produced by the mutual interference of a set of wavefronts) is observed and it is seen to be in constant motion. The rate at which these intensity fluctuations occur is related to

the motion of the particles and thus their size. Small particles cause the intensity to fluctuate more rapidly than large ones [59]. An efficient and common way to measure these intensity fluctuations is by using a digital autocorrelator.

A correlator is basically a signal comparator. It measures the degree of similarity between two signals, or one signal with itself at given time intervals. If the time interval between measurements is relatively long, it is expected that the correlation will be lost; as any other case were a random mechanism is involved (diffusion in this case). However, if the time interval between measurements is small enough, there will be a strong relationship or correlation between the intensities of two signals. Then it can be said that the two signals are strongly, or well correlated. A perfect correlation is indicated by unity and no correlation is indicated by zero. As the time passes the correlation will drop until it eventually reaches a point of no correlation.

The correlator used in a PCS instrument will construct the auto-correlation function of the scattered intensity

$$\langle I(q,0)I(q,t')\rangle = \lim_{T\to 0}\frac{1}{T}\int_0^T I(q,t)I(q,t+t') \tag{1}$$

where *q* is the scattering vector, *I* the intensity, and the *t* the time.

The correlation function measured by the PCS is in reality a normalized version of equation 1

$$g^{(2)}(q,t') = \frac{\langle I(q,0)I(q,t')\rangle}{\langle I(q)\rangle^2} \tag{2}$$

this normalized auto-correlation function can be related to the electric field auto-correlation function $g^{(1)}(q,t')$ with the following equation

$$g^{(2)}(q,t') = 1 + \sigma\left|g^{(1)}(q,t')\right|^2 \tag{3}$$

where σ is an instrumental coherence factor close to 1 for the newest collecting optic systems [59]. The electric field auto-correlation function $g^{(1)}(q,t')$ for Brownian motion of monodisperse spherical nanoparticles is

$$\boldsymbol{g^{(1)}(q,t') = Ae^{-t'/\tau}} \quad (4)$$

In the case the nanoparticles are polydisperse, a correction to equation 4 has to be included.

$$g^{(1)}(q,t') = Ae^{-\left(t'/\tau_{kww}\right)^{\beta}} \quad (5)$$

This is the Kohlrausch-Williams-Watts function (KWW) [59], which make use of a stretched exponential by using a parameter β that varies between $\{0 < \beta < 1\}$.

From the correlation curves different information can be obtained, for example, the time at which the correlation starts to significantly decay is an indication of the mean size of the sample, while the steeper this line decay, the more monodisperse the sample is. Conversely, the more extended the decay becomes, the greater the sample polydispersity. In Figure 8 a correlation plot for the case of Alumina-BMIM-BF_4 is shown.

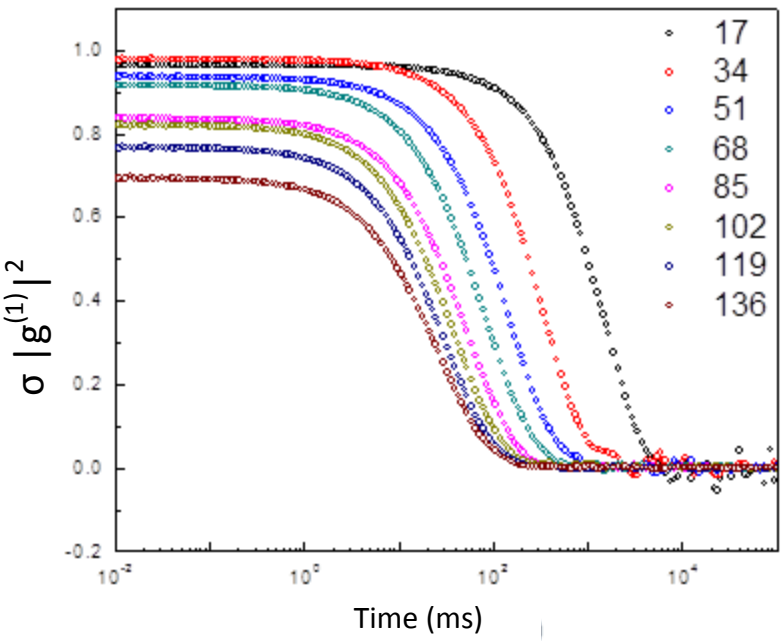

Figure 8. Correlation plot of Alumina-BMIM-BF_4 (0.03 wt%).

Equation 5 is used to fit the measured correlation function shown in Figure 8. Once the fitting parameters are obtained, they can be used to find the average relaxation time $\langle\tau\rangle$ which is a correction to the τ_{KWW} relaxation time [59].

$$\langle\tau\rangle = \int_0^\infty e^{-\left(t'/\tau_{kww}\right)^\beta} dt = \frac{\tau_{KWW}}{\beta}\Gamma(\beta^{-1}) \quad (6)$$

This $\langle\tau\rangle$ can be related to the translational diffusion through the following equation [59],

$$\langle\tau\rangle = (Dq^2)^{-1} \quad (7)$$

where the scattering vector q is given by

$$|q| = q = \frac{4\pi n}{\lambda_0} Sin\frac{\theta}{2} \quad (8)$$

Here θ is the scattering angle, n is the refracting index of the solvent and λ_0 is the wavelength of the incident light. The way the average translational diffusion coefficient is found is simply by plotting $\frac{1}{\langle\tau\rangle}$ vs q^2 and fit to a linear function, see Figure 9. The resulting pendent of the function will be the average translational diffusion coefficient.

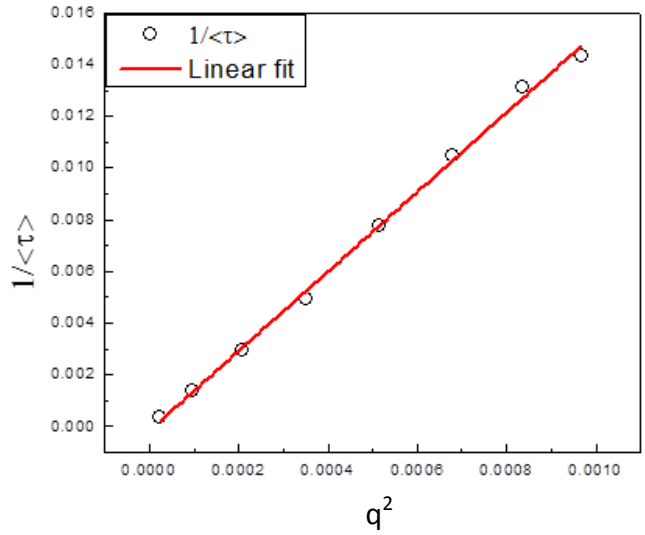

Figure 9. Linear fitting curve used to determine the average diffusion coefficient (data from Figure 8).

The particles size is calculated from the average translational diffusion coefficient by using the Stokes-Einstein equation [59],

$$d = \frac{kT}{3\pi\eta D} \tag{9}$$

where d is the hydrodynamic diameter, D is the average translational diffusion coefficient, k is the Boltzmann constant, T is the absolute temperature, and η is the viscosity of the fluid.

A sketch of the PCS system used is presented in Figure 10.

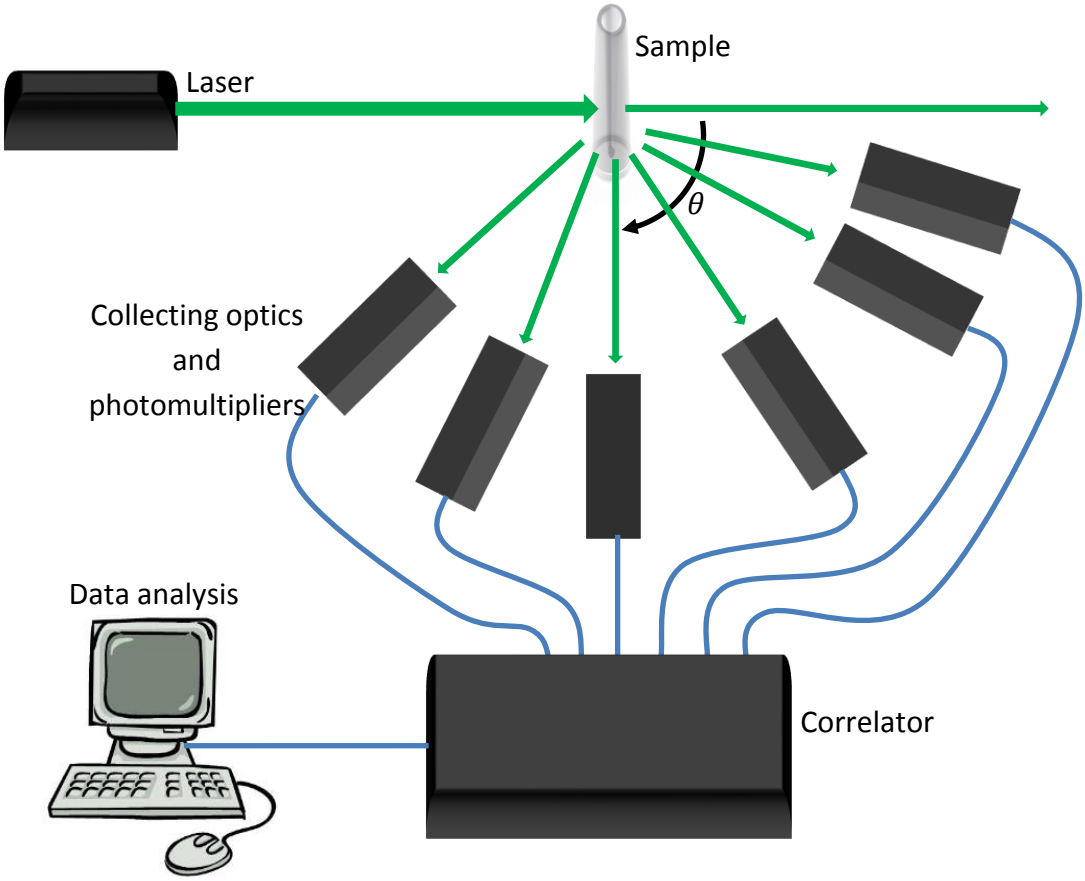

Figure 10. Setup for the PCS experiment.

4.4.3 Dielectric spectroscopy

Dielectric spectroscopy (DS), also known as impedance spectroscopy, measures the dielectric properties of a medium by the interactions of an external field with the electric dipole moment of a given material [60]. DS measurements are often used for characterizing electrochemical systems, by means of measuring the impedance of a system over a range of frequencies. The term impedance is given to

the opposition of flow of alternating current (AC) through a complex system. A passive complex electrical system comprises both an energy dissipater element, better known as a resistor, and energy storage element, known as a capacitor.

In the case of ionic conductivity measurements of an electrolyte material, the cells are usually made of two identical cylindrical electrodes separated by a ring which contains the electrolyte, see Figure 12. The general approach is to apply an electrical stimulus, in our case a voltage, to the electrodes and observe the response, the resulting current. In most experiments it is always assumed that the properties of the electrode material are time-invariant, and therefore stable enough to determine other properties, as a function of temperature, oxygen partial pressure, applied hydrostatic pressure, and applied static voltage. A variety of microscopic processes can take place in the cell and together they lead to the overall electrical response.

When an electric field $\boldsymbol{E}$ is applied to a material, the charges and dipoles will reorient, inducing a polarization $\boldsymbol{P}$ in the material [60]. The relation between the applied electrical field and the polarization of the material is given by

$$\boldsymbol{P} = (\boldsymbol{\varepsilon_r} - \mathbf{1})\boldsymbol{\varepsilon_0}\boldsymbol{E} \tag{10}$$

where ε_0 and ε_r are the permittivity of the vacuum and the material respectively [60]. Assuming that we are working in a linear, homogeneous, isotropic medium and knowing that the relation for the electrical displacement $\boldsymbol{D}$ [60] is given by

$$\boldsymbol{D} = \boldsymbol{\varepsilon_0}\boldsymbol{E} + \boldsymbol{P} \tag{11}$$

it is possible to rewrite the $\boldsymbol{D}$ as only function of ε_r and $\boldsymbol{E}$ by substituting equation 9 on 10

$$\boldsymbol{D} = \boldsymbol{\varepsilon_0}\boldsymbol{\varepsilon_r}\boldsymbol{E} \tag{12}$$

A modulated electrical field $\boldsymbol{E_\omega}(t) = E_0 exp(i\boldsymbol{\omega}t)$ will produce a modulated electrical displacement but with a phase difference due to the response time $\boldsymbol{D_\omega}(t) = D_0 exp\big(i\boldsymbol{\omega}t - i\delta(\boldsymbol{\omega})\big)$. The ratio $\boldsymbol{D_\omega}/\boldsymbol{E_\omega}$ provides the complex variable, the dielectric permittivity, as a function of the frequency $\boldsymbol{\omega}$ [60]**.**

$$\boldsymbol{\varepsilon^*(\omega)} = \boldsymbol{\varepsilon'(\omega)} - \boldsymbol{\varepsilon''(\omega)} = \frac{\boldsymbol{D(\omega)}}{\boldsymbol{\varepsilon_0 E(\omega)}} \tag{13}$$

If a modulated voltage is applied a modulated current will be measure and the complex impedance $\boldsymbol{Z^*(\omega)}$ will be obtained. From $\boldsymbol{Z^*(\omega)}$ it is possible to find the complex dielectric permittivity [60] with the following relationship

$$\boldsymbol{\varepsilon^*(\omega) = \frac{-i}{\omega C_0 Z^*(\omega)}} \tag{14}$$

where C_0 is the empty cell capacitance, which neglecting edge effects is equal to $C_0 = \boldsymbol{\varepsilon_0}\, {}^{A}/_{l}$ where A is the area and l is the distance between electrodes. With equation 14 it is possible to find the ionic conductivity [60] by using the following relation

$$\boldsymbol{\varepsilon^*(\omega) = \varepsilon'(\omega) + i\frac{\sigma}{\omega}} \tag{15}$$

The dc-conductivity can be extracted by plotting the values of $\boldsymbol{\sigma'(\omega)}$ and taking the value of the plateau. If the $\boldsymbol{\sigma'(\omega)}$ is taken at several temperatures the dc-conductivity plot as a function of temperature is generated. In Figure 11 these two graphs are shown.

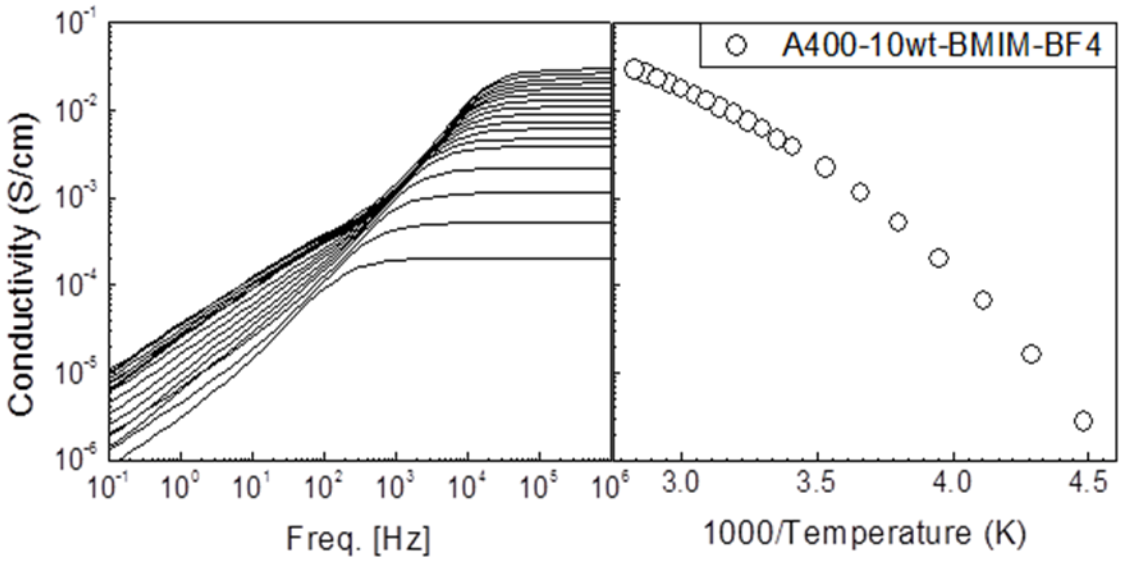

Figure 11. Left, conductivity as a function of frequency for several temperatures. Right, dc-conductivity obtained from the plateau of the left plot as a fuction of temperature. The data comes from measurements on 10 wt% of Aerosil-400 in BMIM-BF_4.

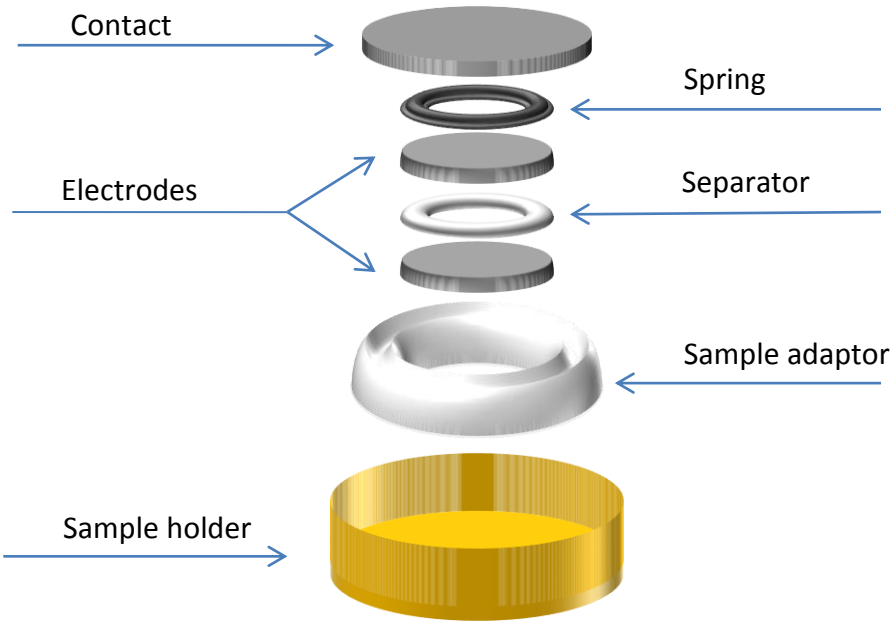

Figure 12. Schematic illustration of the sample container.

4.4.4 Instruments and experimental conditions

The DSC equipment used was a TA Instrument Q1000 coupled with a liquid nitrogen cooling system. The samples, 10-20 mg, were placed in hermetic sealed aluminum pans. The samples were first cooled at a rate of 20 K/min from 313 to 153 K and then heated at a rate of 10 K/min from 153 to 313 K. The data was recorded during the whole experiment and later analyzed with the Universal Analysis 2000 software. The exotherms up convention was used and the T_g was determined using the onset criteria while heating the samples.

The PCS equipment used was an ALV 8000 which make used of a toluene bath in order to decrease static scattering from the vial. Eight detectors were used to collect data at angles from 13 to 155 degrees with respect to the incident beam. The wavelength of the laser was 532 nm. The measurements were done at 298 K.

The ionic conductivity was obtained using a broadband dielectric spectrometer from Novacontrol. The teflon spacer used for the cell had a diameter of 13.1 mm and a thickness of 1 mm. The samples were first heated from 298 to 353 K and then

cooled from 353 to 183 K, using 10 K intervals. The frequency range studied for each temperature step was from 10^{-2} to 10^{7} Hz.

Chapter 5

Results and discussion

5.1 Gelling point

The gelling point of the samples was determined by the simple and practical technique of turning the vials upside down and observing if the sample flows. The nanoparticle concentration when the sample stopped flowing was considered as the gelling point. An example for the case of Aerosil-200/BMIM-BF_4 samples is presented in Figure 13.

Figure 13. Test of the gelling point. From left to right 3, 4, 5, 6 wt% of Aerosil-200 in BMIM-BF_4.

As it can be seen in Figure 13, the nanoparticle concentration where the sample stopped flowing is somewhere between 4 and 6 wt%. Further analysis determined that the gelling point of the Aerosil-200/BMIM-BF_4 mixtures is 5 wt%. The obtained value is rather different from those reported in literature: 3 wt% [16] and 15 wt% [22] respectively. The considerable difference in gelling concentrations might be a result of the techniques used. For the case of 15 wt%, the authors use a rheology experiment where the sample is exposed to the environment, which could be the cause of the different values obtained. Factors that might affect the gelling concentration are purity of the materials, ambient temperature, and water content. The latter is probably the one that affects the most. It is worth to point out that due to the highly hygroscopic character of the BMIM-BF_4, the samples

might absorb water and characteristics such as viscosity and conductivity will be changed depending on the amount of water present in the samples [54].

Figure 14. Liquid/gel phase separation of Aerosil-200/BMIM-BF_4 4 wt% sample.

From Figure 14 it can be observed that a phase separation exist for some samples, i.e. the presence of a liquid and a gel phase. Phase separation at low concentrations has previously not been reported for this system. By systematically increasing the nanoparticle concentration it was possible to observe how the Aerosil-200/BMIM-BF_4 mixtures start to increase viscosity until a point where part of the sample gelled. After this, as the nanoparticle concentration was increased the percentage of sample gelled also increased until a point where the whole sample became a gel. From the concentration where the whole sample is a gel, an increase in concentration will form a stronger gel until the point where the sample becomes a powder. Giving the small yield strength of the samples with concentrations just above the gelling point, it was decided to call them weak-gels.

The gels formed from Aerosil-200/BMIM-BF_4 were stable enough to withstand gravity and small disturbances even in their lower concentrations where the phase separation exists. In Table 5 the state of the different samples of Aerosil-200/BIMM-BF4 are reported.

The same method was used to determine the gelling point of the other nanoparticles/BMIM-BF_4 mixtures. For the case of the Sigma-Aldrich-400/BMIM-BF_4 mixtures, similar results as the ones from Aerosil-200/BMIM-BF_4 mixtures were

found, with a slightly difference in gelling concentration. In Table 6 the states of the different samples of Sigma-Aldrich-400/BMIM-BF_4 are reported.

Table 5. Different states of Aerosil-200/BMIM-BF_4 mixtures.

Aerosil-200 wt% in BMIM-BF_4	**State**
2.5	Liquid
3	Liquid
3.5	Liquid/Gel
4	Liquid/Gel
4.5	Liquid/Gel
5	Weak-Gel
5.5	Gel
6	Gel
6.5	Strong-Gel

Table 6. Different states of Sigma-Aldrich-400/BMIM-BF_4 mixtures.

Sigma-Aldrich-400 wt% in BMIM-BF_4	**State**
4	Liquid
4.5	Liquid
5	Liquid/Gel
5.5	Liquid/Gel
6	Liquid/Gel
6.5	Liquid/Gel
7	Liquid/Gel
7.5	Weak-Gel
8	Gel
9	Strong-Gel

Similar to the Aerosil-200/BMIM-BF_4 gels the Sigma-Aldrich-400/BMIM-BF_4 gels were stable enough to withstand gravity and small disturbances even in their lower concentrations where the phase separation exists.

For the case of the Aeroxide-Alu-C/BMIM-BF_4 mixtures, as expected, the viscosity increase with the increase of nanoparticle concentration. However, no phase separation was observed. Another remarkable difference with respect to the silica nanoparticles, was that the samples became opaque even at low

concentrations (1 wt%) until a point where the samples were completely white. This means that the particle size is close to the visible wavelength or that the nanoparticles are agglomerating into bigger units that again are around the visible range. The Aeroxide-Alu-C/BMIM-BF_4 change from a viscous liquid to a weak gel, which with increasing concentration became a stronger gel, until reaching a point where the mixture becomes a powder. In Table 7 the states of the different samples of Aeroxide-Alu-C/BMIM-BF_4 are reported.

Table 7. Different states of Aeroxide-Alu-C/BMIM-BF_4 mixtures.

Aeroxide-Alu-C wt% in BMIM-BF_4	**State**
4	Liquid
5	Liquid
6	Weak-Gel
7	Weak-Gel
9	Gel
10	Gel
11	Strong-Gel

The gels formed from Aeroxide-Alu-C/BMIM-BF_4 were stable enough to withstand gravity. However, small disturbances, such as gently hitting the vials with the finger, were enough the break the gel state and start the flow. This only happened for the samples characterized as weak-gels. This effect can be seen in Figure 15.

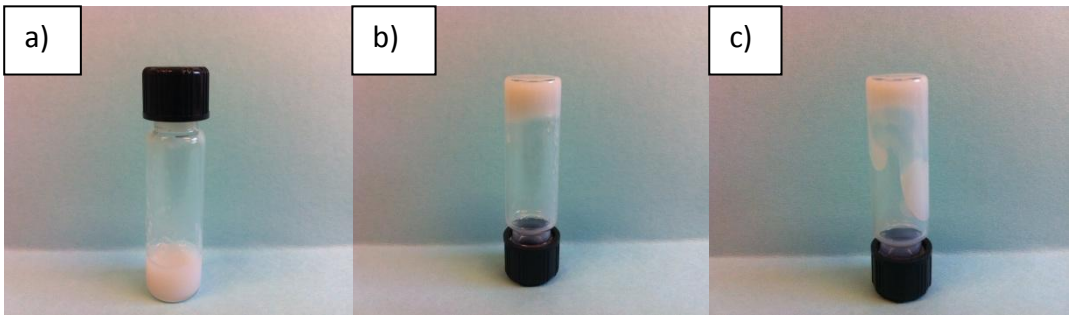

Figure 15. Peculiar weak-gel behavior of Aeroxide-Alu-C/BMIM-BF_4 7 wt% sample. In a) the sample after 2 hours of rest, in b) the sample after 15 minutes of being turned upside down and in c) the sample seconds after a small disturbance.

In the case of samples with higher nanoparticle concentration, the behavior was similar to that of the silica samples.

For the case of Aeroxide-TiO-P25/BMIM-BF_4 mixtures, the particles simply sediment to the bottom of the vials, phase separating from the ionic liquid for any given concentration. Therefore, no further analysis was performed for these mixtures.

Moreover, besides the already mentioned behavior of the different samples, if the samples were heated or rigorously disturbed they all flowed as fluids. In the specific case of silica, for the samples that fall into the category of phase separated, when disturbed they recover a homogeneous appearance, however after 12 hours of rest the samples have phase separated. For the case of the weak-gels, when the samples were sonicated at 80 °C for 20 minutes, they recover their fluid behavior, however as soon as they cool down the samples gel again. Finally, for the case of the strong-gels, they withstand temperatures up to 150 °C without losing the gel behavior, and they only flow under strong disturbances. These are all signatures of a physical gel, which confirms that all the systems are reversible.

Table 8 presents the results of the gelling points for the different nanoparticles. The concentrations are expressed in weight percent of nanoparticles dispersed in the ionic liquid.

Table 8. Gelling concentration of BMIM-BF_4 for different nanoparticles.

Nanoparticle dispersed in BMIM-BF_4	**Gelling concentration (wt%)**
Aerosil-200	5
Sigma-Aldrich-400	7.5
Aeroxide-Alu C	6
Aeroxide-TiO-P25	Sediment

As we can see from Table 8, there are differences in the concentrations of nanoparticles required for gelling. Factors that might play an important role in the colloidal stabilization are particle size, surface area, and interactions between the nanoparticles and the ionic liquid. It has been suggested that the hydroxyl surface

groups of the silica nanoparticles might interact via hydrogen bonding with the Fluorine in BMIM-BF_4 [16, 22]. These interactions might facilitate the formation of layers of anions around the nanoparticles which will induce a solvation force. The solvation force will stabilize the colloidal suspension and prevent the system from gelling. Hence, it is reasonable to think that, due to a higher surface area, there will be a higher number of hydrogen bonds which will sum up to form a more stable layer, resulting in a higher gelling point. From this it can be conclude that for the case of the silica nanoparticles, with increasing surface area the nanoparticle concentration required to gel the ionic liquid is increased.

In the case of the alumina nanoparticles, despite its lower surface area (100 m^2/g), the gelling concentration falls between those of the two different silica nanoparticles. As for the case of silica, the hydroxyl surface groups might interact to form the solvation layers. However, due to the positively charged surface of the alumina and previous suggestions from literature stating the anion is interacting with the alumina surface [61], electrostatic interactions might be contributing to stabilize the solvation layer. Hence, these two mechanisms might be coupling to stabilize the solvation layer, and as a result, withstand higher nanoparticle concentrations. Also the strength of the alumina gel was lower compare to the silica gels. This might be explained by the lower concentration of hydroxyl groups. Since the particles remain together through hydrogen bonding, the less hydroxyl groups on the surface the less hydrogen bonding and the weaker the gel will be. These results display the importance of the surface groups and the way the nanoparticles interact with the ionic liquid and with each other. However, other parameters such as nanoparticle size could be contributing. Due to this uncertainty the particle size will be determined in the following section.

5.2 Particle size

In order to determine the mean diameter of the nanoparticles PCS experiments were performed. The size of the particles was determined for dispersion with concentrations lower than 0.1 wt% to ensure the least possible multiple scattering

events. As a reference, the hydrodynamic diameter of the particles in BMIM-BF_4 was compared with the one of particles dispersed in water. This comparison can determine whether the particles aggregate to bigger particles or not, or until what extend the dispersive fluid is interacting with the nanoparticles. In Figure 16 the plots used to obtain the average translational diffusion coefficient are presented.

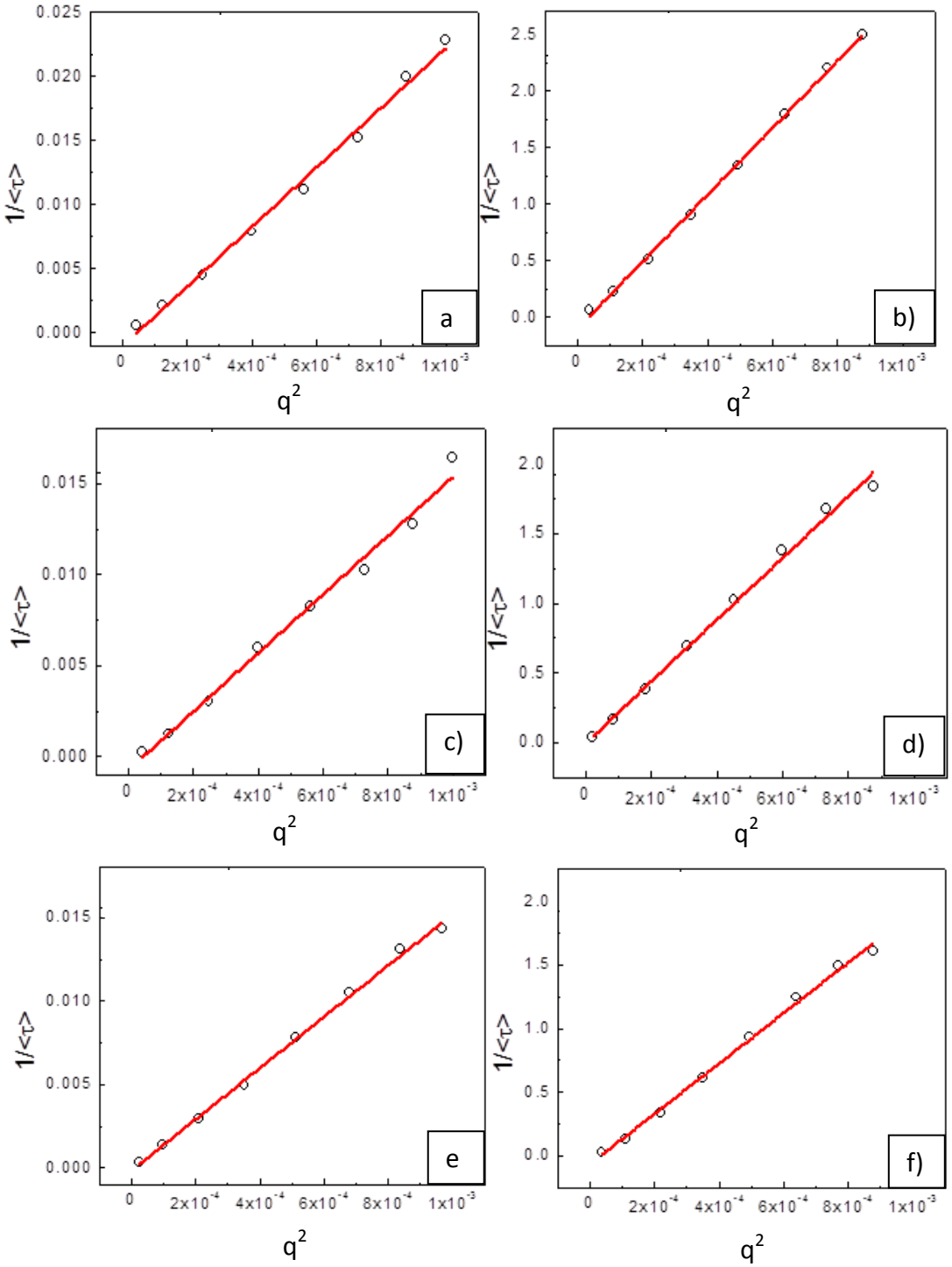

Figure 16. Plots used to extract the average translational diffusion coefficient. On the left side, a), c) and e) correspond to Aerosil-200, Sigma-Aldrich-400 and Aeroxide-Alu-C nanoparticles dispersed in BMIM-BF_4, respectively. Similar in the right side for b), d) and f) in water.

From Figure 16, it can be seen that the data points do not fall far away from the fitting line. This means that the particles are not polydisperse. The diameter found by using the average translational diffusion coefficient for the case of the BMIM-BF_4 might be over or sub-estimated depending on the amount of water present. For these reason in Table 9 the mean hydrodynamic diameter of the different nanoparticles dispersed in BMIM-BF_4 and water is presented, together with their respective diffusion coefficients.

Table 9. Mean hydrodynamic diameters and diffusion coefficients of the different nanoparticles in BMIM-BF_4.

Nanoparticles	**Water**		**BMIM-BF_4**	
	Diffusion coefficient $10^{-11}(cm^2/s)$	**Diameter (nm)**	**Diffusion coefficient $10^{-11}(cm^2/s)$**	**Diameter (nm)**
Aerosil-200	2953	166	23	189
Sigma-Aldrich-400	2212	222	16	273
Aeroxide-Alu-C	1979	247	15	287

From Table 9, it can be seen that the hydrodynamic diameter of the particles in BMIM-BF_4, compared to the diameter found in water, does not vary to a point that considerable particle aggregation could be considered. Using as aggregation criteria that the size measured in BMIM-BF_4 has to be at least twice the one measured on water. It is important to point out that the viscosity used to calculate the diameter of the particles was taken from literature [54] and not directly measured from the ionic liquid used here. This uncertainty might account for some deviation in the actual diameter of the nanoparticles in the BMIM-BF_4.

5.3 Ionic conductivity and glass transition temperature

The ionic conductivity of the different samples is reported in conductivity vs temperature graphs. For all the different nanoparticles used, two plots will be presented: first, how the conductivity varies as a function of temperature, and second, how the conductivity varies as a function of nanoparticles concentration at

room temperature. Figure 17 shows the ionic conductivity plots for all the nanoparticles studied.

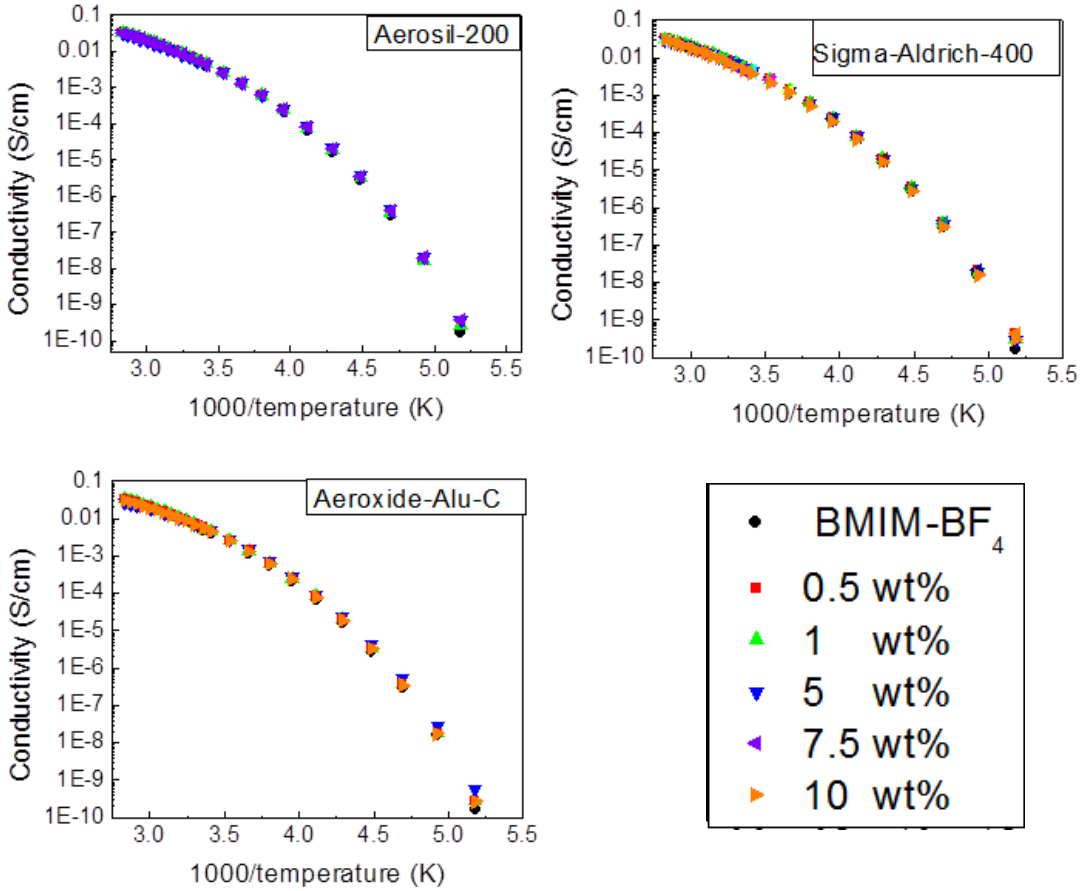

Figure 17. Ionic conductivity as a function of temperature.

The measured ionic conductivity of BMIM-BF_4 is in good agreement with those reported in literature [14, 52]. The ionic conductivity at room temperature found is 4.9 mS/cm. From Figure 17 it is seen that the conductivity does no vary considerably with nanoparticle concentration for the temperature range studied. Similar results have been found for other ionic liquids [20, 21]. This suggests that the ionic liquid, even though the sample is a gel, does not interact in a strong way with the nanoparticles and it is simply contained in the network. The ionic liquid can freely move inside the fractal structure formed by the nanoparticles. This is a good result, since it is possible to combine the advantageous mechanical properties of the gels without degrading the transport properties of the ionic liquids.

The changes in ionic conductivity with respect to nanoparticle concentration are relatively small. In order to have a more detailed picture, in Figure 18 the ionic conductivity for the different nanoparticles at room temperature is presented.

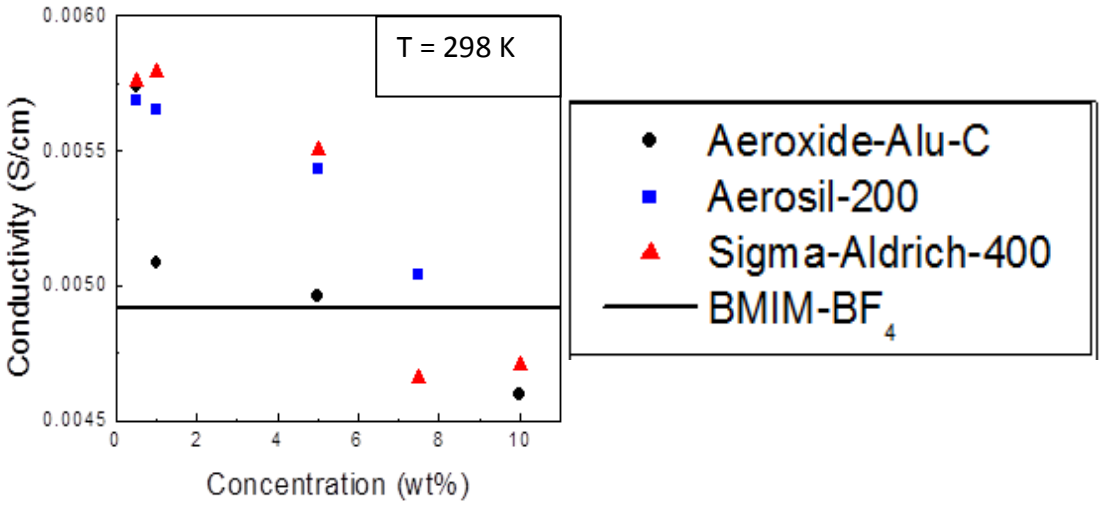

Figure 18. Ionic conductivity as a function of nanoparticle concentration at room temperature.

From Figure 18 it is possible to see that at low nanoparticle concentration, the ionic conductivity is slightly higher than the one of the pure ionic liquid. This might be a result of the impurities of the nanoparticles, which could be contributing ions to slightly enhance the ionic conductivity. Moreover, a slow decrease in conductivity when the nanoparticle concentration is increased can be observed. This could be explain by the nanoparticle network formed, with small nanoparticles concentrations, the ionic liquid can freely move in the dispersion, however, as the nanoparticle concentration increase, the network will start to obstruct the movement of the ionic liquid, causing a decrease in conductivity. Furthermore, Figure 18 shows that the alumina nanoparticles-BMIM-BF_4 dispersions, tend to decrease the ionic conductivity as a function of nanoparticle concentration slightly faster than the silica nanoparticles, thought this change is not completely clear given that the lower and higher concentrations present similar conductivity as those of the silica dispersions.

As an additional result, Table 10 reports values for the glass transition temperatures of the ionic liquid determined from DSC experiments for the pure ionic liquid and for the gelled samples.

Table 10. Glass transition temperature of gelled samples and pure BMIM-BF_4.

Samples	**Glass transition temperature (K)**
Pure-BMIM-BF_4	186.0
Aerosil-200-7.5wt%/BMIM-BF_4	186.1
Aerosil-400-10wt%/BMIM-BF_4	186.1
Aeroxide-Alu-C-10wt%/BMIM-BF_4	185.4

As it can be seen in Table 10, there are no significant changes between the pure ionic liquid and the gelled samples. This suggests that the interaction between the ionic liquid and the nanoparticles is weak and therefore does not significantly change the structure or dynamics of the pure ionic liquid.

The small changes in ionic conductivity together with the lack of variation of the glass transition temperature confirm that the interaction nanoparticles-BMIM-BF_4 is weak.

Chapter 6

Conclusions

The silica and alumina nanoparticles were able to form gels with BMIM-BF_4, whereas the titanium oxide nanoparticles simply sediment. For the case of silica nanoparticles, the combination of larger particle size and higher surface area, results in higher gelling concentrations. For the alumina nanoparticles, despite the larger particle size and the low surface area, the gelling concentration falls between those of the silica nanoparticles. This can be explained by the mixed contribution of hydrogen bonding and electrostatic interaction between the positively charge surface of alumina and the anion BF_4. The gels formed from silica nanoparticles are stronger than the ones from alumina. This can be related to the amount of hydroxyl surface groups determining how strong the gels are. Also the nanoparticle concentration determines the strength of the gels. With low concentration the gels have lower yield strength (weak-gels) as the nanoparticle concentration increase the yield strength increase (strong-gels).

The ionic conductivity of the BMIM-BF_4 and the colloidal dispersions were reported for a temperature range from 193 K to 353 K. The conductivity values obtained for BMIM-BF_4 are in good agreement with those reported in literature. The ionic conductivity of the colloidal dispersions studied slightly decrease with nanoparticle concentration. These results are in line with similar studies reported for other ionic liquids. The glass transition temperature and ionic conductivity of the nanoparticle/BMIM-BF_4 mixtures does not vary considerably over the range of nanoparticle concentrations (0-10 wt%) and temperatures studied (193-353 K). Even though the samples behave as solid-like materials (Gel) the ionic conductivity remains relatively unchanged with respect to the pure ionic liquid.

Further work

In order to complement this thesis some further studies are required. For instance the study of silica and alumina nanoparticles with other surface areas could provide a more detailed picture of the stabilization mechanism present in the colloidal suspensions. Furthermore, vibrational spectroscopy methods (Raman spectroscopy) could provide an inside look of the surface interactions present between the BMIM-BF_4 and the nanoparticles. Finally, similar studies with other ionic liquids will be helpful to compare the way the ionic liquid-nanoparticle systems interact and whether or not the systems behave as expected.

Akcnowledgements

First, I would like to express my gratitude to my supervisor Professor Aleksandar Matic for the continuous support and guidance during my thesis work. Special thanks to PhD students Jonas Nordström and Jagatth Pitawala for their close support and guidance through the experimental techniques. And in general, to the entire Condensed Matter Physics group that provide a friendly and enjoyable work environment.

Secondly, I would like to thank the European Commission for the financial support through the Erasmus Mundus Master program. Extend my gratitude to all the great people that I meet during the program, in special to Esteban Rucavado who worked with me in close collaboration during the whole thesis project.

Finally, I would like to thank my family who has giving me the strength to pursue my dreams and support during my entire life.

Bibliography

1. Lee, S.W., et al., *High-power lithium batteries from functionalized carbon-nanotube electrodes.* Nat Nano, 2010. **5**(7): p. 531-537.

2. Bruce, P.G., B. Scrosati, and J.-M. Tarascon, *Nanomaterials for Rechargeable Lithium Batteries.* Angewandte Chemie International Edition, 2008. **47**(16): p. 2930-2946.

3. Armand, M. and J.M. Tarascon, *Building better batteries.* Nature, 2008. **451**(7179): p. 652-657.

4. Zhou, X., et al., *Graphene modified LiFePO4 cathode materials for high power lithium ion batteries.* Journal of Materials Chemistry, 2011. **21**(10): p. 3353-3358.

5. Tarascon, J.M. and M. Armand, *Issues and challenges facing rechargeable lithium batteries.* Nature, 2001. **414**(6861): p. 359-367.

6. Kim, G.-H., A. Pesaran, and R. Spotnitz, *A three-dimensional thermal abuse model for lithium-ion cells.* Journal of Power Sources, 2007. **170**(2): p. 476-489.

7. Spotnitz, R.M., et al., *Simulation of abuse tolerance of lithium-ion battery packs.* Journal of Power Sources, 2007. **163**(2): p. 1080-1086.

8. Harris, S.J., A. Timmons, and W.J. Pitz, *A combustion chemistry analysis of carbonate solvents used in Li-ion batteries.* Journal of Power Sources, 2009. **193**(2): p. 855-858.

9. Arbizzani, C., G. Gabrielli, and M. Mastragostino, *Thermal stability and flammability of electrolytes for lithium-ion batteries.* Journal of Power Sources, 2011. **196**(10): p. 4801-4805.

10. Fredlake, C.P., et al., *Thermophysical Properties of Imidazolium-Based Ionic Liquids.* Journal of Chemical & Engineering Data, 2004. **49**(4): p. 954-964.

11. Paulechka, Y.U., et al., *Vapor pressure and thermal stability of ionic liquid 1-butyl-3-methylimidazolium Bis(trifluoromethylsulfonyl)amide.* Thermochimica Acta, 2005. **439**(1-2): p. 158-160.

12. Aschenbrenner, O., et al., *Measurement of vapour pressures of ionic liquids and other low vapour pressure solvents.* Green Chemistry, 2009. **11**(8): p. 1217-1221.

13. Stoppa, A., et al., *The Conductivity of Imidazolium-Based Ionic Liquids from (−35 to 195) °C. A. Variation of Cation's Alkyl Chain†.* Journal of Chemical & Engineering Data, 2009. **55**(5): p. 1768-1773.

14. Yu, Y.-H., A.N. Soriano, and M.-H. Li, *Heat capacities and electrical conductivities of 1-n-butyl-3-methylimidazolium-based ionic liquids.* Thermochimica Acta, 2009. **482**(1-2): p. 42-48.

15. Nakagawa, H., et al., *Application of nonflammable electrolyte with room temperature ionic liquids (RTILs) for lithium-ion cells.* Journal of Power Sources, 2007. **174**(2): p. 1021-1026.

16. Hong Yang, C.Y., Qunliang Song, Yongyao Xia, Fuyou Li, Zhigang Chen, Xianghong Li, Tao Yi, and Chunhui Huang, *High-Temperature and Long-Term Stable Solid-State Electrolyte for Dye-Sensitized Solar Cells by Self-assembly.* Chem. Mater., 2006. **18**(22): p. 5173-5177.

17. Thamarai Devarajan, S.H., Christopher Dangler, Manisha Rane-Fondacaro, Jeremy Snyder and Pradeep Halda, *Novel ionic liquid electrolyte for electrochemical double layer capacitors.* Electrochemistry Communications, 2009. **11**: p. 680-683.

18. Katsuhiko Tsunashima, F.Y.a.M.S., *A Lithium Battery Electrolyte Based on a Room-temperature Phosphonium Ionic Liquid.* Chemistry letters, 2008. **37**(3): p. 314.

19. Armand, M., et al., *Ionic-liquid materials for the electrochemical challenges of the future.* Nat Mater, 2009. **8**(8): p. 621-629.

20. Kazuhide Ueno, K.H., Toru Katakabe, Masashi Kondoh and Masayoshi Watanabe, *Nanocomposite Ion Gels Based on Silica Nanoparticles and an Ionic Liquid: Ionic Transport, Viscoelastic Properties, and Microstructure.* J. Phys. Chem. B, 2008. **112**(30): p. 9013-9019.

21. Toru Katakabe, R.K., and Masayoshi Watanabe, *Acceleration of Redox Diffusion and Charge-Transfer Rates in an Ionic Liquid with Nanoparticle Addition.* Electrochemical and Solid-State Letters, 2007. **10**(6): p. F23-F25.

22. Ueno, K., et al., *Colloidal Interaction in Ionic Liquids: Effects of Ionic Structures and Surface Chemistry on Rheology of Silica Colloidal Dispersions.* Langmuir, 2009. **25**(2): p. 825-831.

23. Ueno, K., et al., *Colloidal Stability of Bare and Polymer-Grafted Silica Nanoparticles in Ionic Liquids.* Langmuir, 2008. **24**(10): p. 5253-5259.

24. Everett, D.H., *Manual of Symbols and Terminology for Physicochemical Quantities and Units, Appendix II: Definitions, Terminology and Symbols in Colloid and Surface Chemistry.* 1972. **31**(4): p. 577-638.

25. Israelachvili, J.N., *Intermolecular and Surface Forces*. Thirth Edition ed2011: Elsevier.

26. J. Alemán, A.V.C., J. He, M. Hess, K. Horie, R. G. Jones, P. Kratochvíl, I. Meisel, I. Mita, G. Moad, S. Penczek and R. F. T. Stepto, *Definitions of terms relating to the structure and processing of sols, gels, networks, and inorganic-organic hybrid materials.* 2007. **79**(10): p. 1801-1829.

27. Kajiwara, Y.O.a.K., *Gels Handbook - Volume 1 - The fundamentals*2001, London, UK: Academic Press.

28. Freemantle, M., *An introduction to ionic Liquids*2010, Cambridge, UK: The Royal Society of Chemistry.

29. Gorlov, M. and L. Kloo, *Ionic liquid electrolytes for dye-sensitized solar cells.* Dalton Transactions, 2008(20): p. 2655-2666.

30. de Souza, R.F., et al., *Room temperature dialkylimidazolium ionic liquid-based fuel cells.* Electrochemistry Communications, 2003. **5**(8): p. 728-731.

31. Seki, S., et al., *Imidazolium-Based Room-Temperature Ionic Liquid for Lithium Secondary Batteries.* Journal of The Electrochemical Society, 2007. **154**(3): p. A173-A177.

32. Horn, R.G. and J.N. Israelachvili, *Direct measurement of structural forces between two surfaces in a nonpolar liquid.* The Journal of Chemical Physics, 1981. **75**(3): p. 1400-1411.

33. Mizukami, M., K. Kusakabe, and K. Kurihara, *Shear resonance measurement on structuring of liquids confined between mica surfaces*, in *Surface and Colloid Science*, F. Galembeck, Editor 2004, Springer Berlin / Heidelberg. p. 105-108.

34. Israelachvili, J.N. and R.M. Pashley, *Molecular layering of water at surfaces and origin of repulsive hydration forces.* Nature, 1983. **306**(5940): p. 249-250.

35. Israelachvili, J. and H. Wennerstrom, *Role of hydration and water structure in biological and colloidal interactions.* Nature, 1996. **379**(6562): p. 219-225.

36. Atkin, R. and G.G. Warr, *Structure in Confined Room-Temperature Ionic Liquids.* The Journal of Physical Chemistry C, 2007. **111**(13): p. 5162-5168.

37. Hayes, R., G.G. Warr, and R. Atkin, *At the interface: solvation and designing ionic liquids.* Physical Chemistry Chemical Physics, 2010. **12**(8): p. 1709-1723.

38. Horn, R.G., D.F. Evans, and B.W. Ninham, *Double-layer and solvation forces measured in a molten salt and its mixtures with water.* The Journal of Physical Chemistry, 1988. **92**(12): p. 3531-3537.

39. Min, Y., et al., *Measurement of Forces across Room Temperature Ionic Liquids between Mica Surfaces.* The Journal of Physical Chemistry C, 2009. **113**(37): p. 16445-16449.

40. Perkin, S., T. Albrecht, and J. Klein, *Layering and shear properties of an ionic liquid, 1-ethyl-3-methylimidazolium ethylsulfate, confined to nano-films between mica surfaces.* Physical Chemistry Chemical Physics, 2010. **12**(6): p. 1243-1247.

41. Ueno, K., et al., *Resonance shear measurement of nanoconfined ionic liquids.* Physical Chemistry Chemical Physics, 2010. **12**(16): p. 4066-4071.

42. Pinilla, C., et al., *Structure and Dynamics of a Confined Ionic Liquid. Topics of Relevance to Dye-Sensitized Solar Cells.* The Journal of Physical Chemistry B, 2005. **109**(38): p. 17922-17927.

43. Sha, M., et al., *Double-Layer Formation of [Bmim][PF6] Ionic Liquid Triggered by Surface Negative Charge.* Langmuir, 2010. **26**(15): p. 12667-12672.

44. Smith, J.A., et al., *Surprising Particle Stability and Rapid Sedimentation Rates in an Ionic Liquid.* The Journal of Physical Chemistry Letters, 2009. **1**(1): p. 64-68.

45. Ueno, K. and M. Watanabe, *From Colloidal Stability in Ionic Liquids to Advanced Soft Materials Using Unique Media.* Langmuir, 2011: p. null-null.

46. Gutsch, A., H. Mühlenweg, and M. Krämer, *Tailor-Made Nanoparticles via Gas-Phase Synthesis.* Small, 2005. **1**(1): p. 30-46.

47. Parks, G.A., *The Isoelectric Points of Solid Oxides, Solid Hydroxides, and Aqueous Hydroxo Complex Systems.* Chemical Reviews, 1965. **65**(2): p. 177-198.

48. Parfitt, G.D., *Surface Chemistry of Oxides*, in *International Conference on Colloid and Surface Science*, P.a.A. Chemistry, Editor 1976: Budapest, Hungary. p. 415-418.

49. Peri, J.B., *A Model for the Surface of γ-Alumina1.* The Journal of Physical Chemistry, 1965. **69**(1): p. 220-230.

50. Brady, P.V., *Alumina surface chemistry at 25, 40, and 60 °C.* Geochimica et Cosmochimica Acta, 1994. **58**(3): p. 1213-1217.

51. Tsyganenko, A.A. and P.P. Mardilovich, *Structure of alumina surfaces.* Journal of the Chemical Society, Faraday Transactions, 1996. **92**(23): p. 4843-4852.

52. Nishida, T., Y. Tashiro, and M. Yamamoto, *Physical and electrochemical properties of 1-alkyl-3-methylimidazolium tetrafluoroborate for electrolyte.* Journal of Fluorine Chemistry, 2003. **120**(2): p. 135-141.

53. Liu, W., et al., *The Physical Properties of Aqueous Solutions of the Ionic Liquid [BMIM][BF_4].* Journal of Solution Chemistry, 2006. **35**(10): p. 1337-1346.

54. Rilo, E., et al., *Electrical Conductivity and Viscosity of Aqueous Binary Mixtures of 1-Alkyl-3-methyl Imidazolium Tetrafluoroborate at Four Temperatures†.* Journal of Chemical & Engineering Data, 2009. **55**(2): p. 639-644.

55. Waliszewski, D., et al., *Heat capacities of ionic liquids and their heats of solution in molecular liquids.* Thermochimica Acta, 2005. **433**(1-2): p. 149-152.

56. Bou Malham, I. and M. Turmine, *Viscosities and refractive indices of binary mixtures of 1-butyl-3-methylimidazolium tetrafluoroborate and 1-butyl-2,3-dimethylimidazolium tetrafluoroborate with water at 298 K.* The Journal of Chemical Thermodynamics, 2008. **40**(4): p. 718-723.

57. Zhou, Q., L.-S. Wang, and H.-P. Chen, *Densities and Viscosities of 1-Butyl-3-methylimidazolium Tetrafluoroborate + H2O Binary Mixtures from (303.15 to 353.15) K.* Journal of Chemical & Engineering Data, 2006. **51**(3): p. 905-908.

58. Gabbott, P., ed. *Principles and Applications of Thermal Analysis*. First ed. 2008, Blackwell Publishing Ltd.

59. Pecora, B.J.B.a.R., *Dynamic Light Scattering with applications to chemistry, biology, and physics*1975: John Wiley.

60. Schonhals, F.K.a.A., *Broadband dielectric spectroscopy*2003, Berlin, Germany: Springer.

61. Robert Carper, W., P. Wahlbeck, and N. Nooruddin, *Semi-Empirical Molecular Modeling of Ionic Liquid Tribology: Ionic Liquid–Aluminum Oxide Surface Interactions.* Tribology Letters, 2011. **43**(2): p. 163-168.